JOURNAL OF CATALYSIS 153, 232–238 (1995)

Ru Clusters with Controlled Sizes in NaY Zeolite: Catalytic Activity for Ethane Hydrogenolysis and XANES

Ihl Hyun Cho,* Sung June Cho,† Seung Bin Park,* and Ryong Ryoo†

*Department of Chemical Engineering and †Department of Chemistry and Center for Molecular Science, Korea Advanced Institute of Science and Technology, Taeduk Science Town, Taejon, 305-701 Korea

Received June 21, 1994; revised November 15, 1994

Ruthenium clusters trapped in the supercage of NaY zeolite were prepared by the reduction of Ru under flowing H_2 at 623 K after a ruthenium-red complex was ion-exchanged into the supercage and subsequently decomposed under vacuum at 673 K. The cluster size was controlled by the heating rate used for the thermal decomposition, and the number of Ru atoms per cluster was estimated using a xenon adsorption technique. Various Ru/NaY samples in which the number of Ru atoms per cluster ranged from 20 to 60 have been used to investigate the effects of a decrease in Ru cluster size on the catalytic reaction rate of ethane hydrogenolysis. The reaction rates per surface Ru atom of a Ru/NaY cluster as compared with the bulk metal surface were approximately two orders of magnitude smaller, and the X-ray absorption near edge structure (XANES) taken at the Ru *K* edge ($1s \rightarrow 4d$ transition) showed an energy shift. However, in spite of cluster size variation within the supercage, the reaction rates per surface Ru atom and the XANES did not change significantly. The activation energy for the reaction was similar for all Ru samples. These results indicate no significant electronic effects on catalytic activity as the cluster size decreased. © 1995 Academic Press, Inc.

INTRODUCTION

Ion exchange of Group 8 metals into zeolite cages followed by the reduction with H_2 at high temperature is a convenient way to obtain small metal clusters trapped in zeolite cages (1). Such a small metal cluster consisting of only a few metal atoms is of interest in catalysis as the cluster approaches the borderline between homogeneous and heterogeneous catalyst (2). The correlation between the rate of catalytic reaction taking place over the cluster and the number of atoms per cluster in this borderline area is worthy of detailed study.

Recently, Ryoo *et al.* (3–8) investigated Group 8 metal clusters in the supercage of faujasite-type zeolites with ^{129}Xe NMR, EXAFS, and xenon adsorption. The cluster size of Pt, Pd, and Ir was difficult to control to a size smaller than that which filled up the supercage, probably due to the metal–support interactions. Ruthenium in NaY zeolite (Ru/NaY) was a unique case where the average cluster size was controllable within the size of the supercage (4). The ruthenium was ion-exchanged as a ruthenium-red complex (9) into the zeolite and decomposed under vacuum at 673 K before the reduction to metal cluster under flowing H_2 at 623 K. Cho *et al.* (4) used a xenon adsorption technique to estimate the number of Ru atoms per cluster. The number of Ru atoms per cluster ranged from 20 to 60 depending on the heating rate for the thermal decomposition.

In this work, we have investigated the effects of the change in the Ru/NaY cluster size on the catalytic activity for ethane hydrogenolysis. We have also measured the X-ray absorption near edge structure (XANES) in order to obtain a better understanding of the impact of the electronic structure on the cluster's catalytic activity.

EXPERIMENTAL

The Ru/NaY catalysts were prepared according to a procedure reported by Cho *et al.* (4). In short, NaY zeolite powder was slurried in 3.14×10^{-3} *M* aqueous solution of NH_3 (28%, Junsei Chemical Co., 100 ml per g NaY) containing $RuCl_3$ (Johnson Matthey, 48.73% Ru, 0.065 g per g NaY) at 330 K, until the zeolite turned purple due to the formation of a ruthenium-red complex (9) ion in the zeolite supercage. The sample was filtered, washed, and dried in a vacuum oven at room temperature (RT). About 0.50 g of this Ru/NaY precursor was placed in a Pyrex U-tube flow reactor that was joined to a xenon NMR tube (3, 4). The sample was evacuated while being heated to 673 K, reduced under flowing H_2 at 623 K, and subsequently evacuated at 673 K. The sample, except for about 50 mg, was transferred to the NMR tube, sealed off with a flame, and used for ^{129}Xe NMR, hydrogen chemisorption, and xenon adsorption measurements as described earlier (3, 4). The remaining sample in the reactor was used for the ethane hydrogenolysis reaction. The weight of the sample was precisely measured after all

0021-9517/95 $6.00

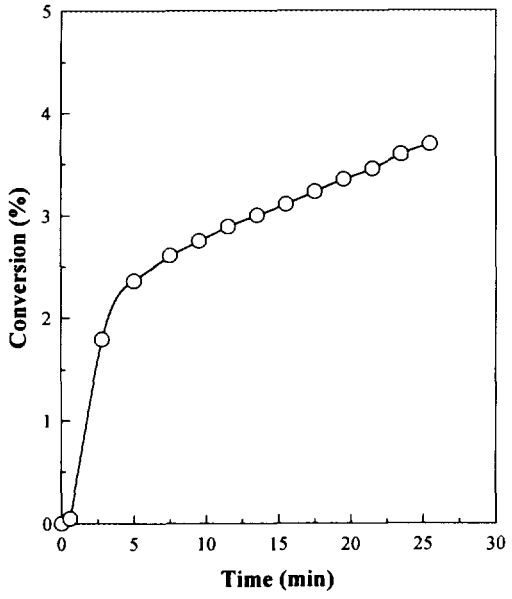

FIG. 1. Conversion of ethane to methane over Ru/NaY, plotted against the reaction time.

experiments were finished. The Ru content determined from elemental analysis was four Ru atoms per unit cell of zeolite.

The rate of ethane hydrogenolysis reaction was measured using a Pyrex batch recirculation system similar to the one described by Schlatter and Boudart (10). The reaction conditions were as follows: $P_{C_2H_6}$ = 3.3 kPa, P_{H_2} = 20 kPa, and P_{He} = 78 kPa. The total volume of the system was 1500 ml. The gas recirculation rate was 3450 ml min^{-1}. The reaction temperature was controlled to within ±1 K in the range 410–460 K. Helium (Korea Industrial Gas, 99.999%) and H_2 (Matheson, UHP grade) were passed through 3A molecular sieve zeolite and MnO/silica traps before use. Ethane (Matheson, 99.5%) was purified by freeze–vacuum–thaw cycles to 99.9+%. The product was analyzed by gas chromatography (HP5890 SERIES II) equipped with a Porapak Q column and a flame ionization detector (FID).

The total conversion of ethane was maintained below 5% to measure the initial reaction rate. The number of ethane molecules per surface Ru atom was plotted against the reaction time. The catalytic activity was taken as an almost constant slope after about one ethane molecule was converted per surface Ru atom, as shown in Fig. 1.

For XANES, 0.25 g of the Ru/NaY precursor was pressed into a self-supporting wafer with a 10 mm diameter. The sample wafer was placed in a Pyrex reactor that was joined to an EXAFS cell. Kapton (125 μm, Du Pont) film was glued as X-ray windows to the EXAFS cell using Torr Seal (Varian). Xenon adsorption was measured after the sample wafer was treated to generate Ru clusters. The sample wafer was then transferred into the X-ray adsorption cell and sealed off under a H_2 atmosphere with flame. The X-ray absorption was measured at the Ru *K* edge at room temperature using Beam Line 10B of the Photon Factory in Tsukuba. The beam injection energy was 2.5 GeV, and the ring current was maintained as 300–330 mA. The energy was scanned at a 0.5-eV interval using a Si(311) channel cut monochromator. The X-ray absorption was measured using two ionization chambers.

RESULTS

^{129}Xe NMR Spectra

All ^{129}Xe NMR spectra were obtained under 53.3 kPa and 296 K. The chemical shift and linewidth were very similar to those reported previously (4). Figure 2a was obtained from a Ru/NaY sample which was reduced at 623 K after evacuation at 673 K. Figure 2b was obtained from NaY zeolite after evacuation at 673 K. The chemical shift in Fig. 2a was higher than in Fig. 2b, and this was in good agreement with the chemical shift increase due to xenon adsorbed on small Ru clusters. Figure 2c was obtained after the above Ru/NaY sample was heated in O_2 for 1 h at 573 K and reduced again. The chemical shift decreased to a value similar to that of NaY zeolite. This chemical shift change is known to result from agglomeration of the small Ru clusters in a supercage into large

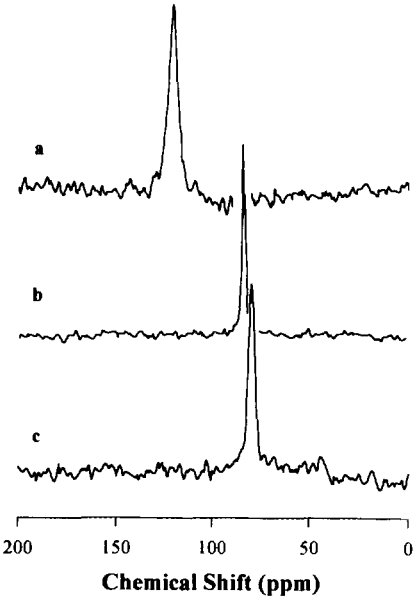

FIG. 2. ^{129}Xe NMR spectra of (a) Ru/NaY reduced at 623 K after evacuation at 673 K, (b) NaY zeolite evacuated at 673 K, and (c) Ru/NaY reduced again after heating in O_2 at 573 K. All the spectra were obtained at xenon pressure of 53.3 kPa at 296 K.

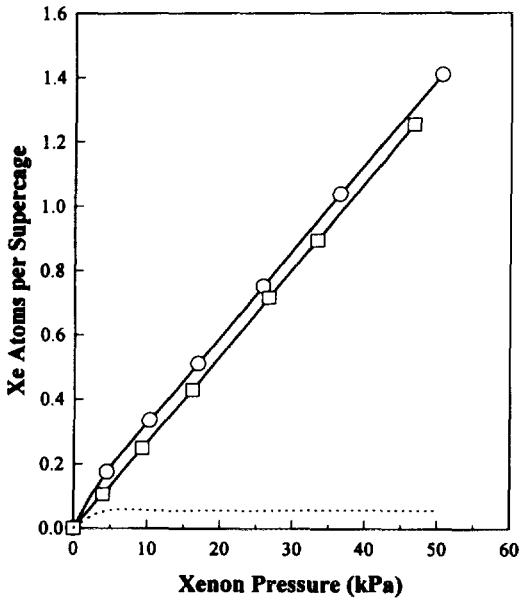

FIG. 3. Xenon adsorption isotherms for Ru/NaY at 296 K: (○) fresh Ru/NaY sample; (□) Ru/NaY with chemisorbed oxygen; (·····) difference between the two isotherms.

particles located on external surface of the zeolite crystal during heating in O_2 (4). Ryoo *et al.* showed that such a heat treatment of Ru/NaY in O_2 at high temperature caused the formation of large Ru particles on the external surface of the zeolite crystal, of dimensions 100 nm × 20 nm (3).

Xenon Adsorption Isotherm and Number of Ru Atoms per Cluster

Two xenon adsorption isotherms were obtained at 296 K for each Ru/NaY sample, as shown in Fig. 3. One adsorption isotherm was obtained from a Ru/NaY sample with an adsorbate-free surface. The other was obtained after the sample was equilibrated with O_2 for 30 min at 296 K and subsequently evacuated for 1 h at 296 K. The dashed line in Fig. 3 represents the difference between the two adsorption isotherms. As Cho *et al.* reported (4), the xenon adsorption isotherm for a clean surface can be separated into a xenon adsorption isotherm for the Ru surface and another isotherm for the zeolite wall. Chemisorption of O (oxygen atoms) on Ru inhibits the xenon adsorption on Ru clusters. Hence, the xenon adsorption isotherm on a surface with chemisorbed O measures the xenon adsorption isotherm on the zeolite wall. The difference in adsorption isotherm in Fig. 3 therefore measures the xenon adsorption isotherm for the Ru surface.

The dashed line in Fig. 3 shows that the xenon adsorption became almost saturated at 5 kPa. The quantity of xenon adsorption for saturation on Ru was obtained by extrapolating a high-pressure linear part of the dashed line to zero pressure. The results thus obtained are given in Table 1 in terms of a Xe/Ru ratio. The Xe/Ru ratio depended on the heating rate used for evacuation of the Ru/NaY precursor. The number of Ru atoms per cluster can be obtained using a space-filling model for the xenon adsorption on Ru clusters trapped in the supercage. This procedure is fully described elsewhere (3–8). Determination of the number of Ru atoms per cluster by this xenon adsorption method gave results ranging from 20 to 60 atoms per cluster, as listed in Table 1.

TABLE 1

Xenon Adsorption on Ru/NaY and the Number of Ru Atoms per Cluster[a]

Sample no.	Xe/Ru	n^b	% Surface atoms[c]
1	0.159	25	0.96
2	0.137	29	0.93
3	0.112	36	0.89
4	0.099	40	0.88
5	0.096	42	0.83
6	0.076	53	0.77
7	0.074	54	0.76

[a] Four Ru atoms per unit cell of Y zeolite.
[b] Average number of Ru metal atoms per cluster.
[c] Determined from the space-filling model.

Ethane Hydrogenolysis

The rate of ethane hydrogenolysis reaction was measured with the Ru/NaY samples listed in Table 2. The results are plotted against the number of Ru atoms per cluster in Fig. 4. The catalytic activity is expressed as the number of converted ethane molecules per second per

TABLE 2

Catalytic Reaction Rate and the Activation Energy of Ethane Hydrogenolysis over Ru/NaY

n	$\nu \times 10^{4a}$	E_a (kcal · mol^{-1})
25	3.4	32
29	3.6	40
36	5.7	39
40	5.5	41
42	5.5	41
53	4.6	46
54	5.1	37
∞	64.1	35

[a] ν represents the number of ethane molecules converted per surface Ru atom per second.

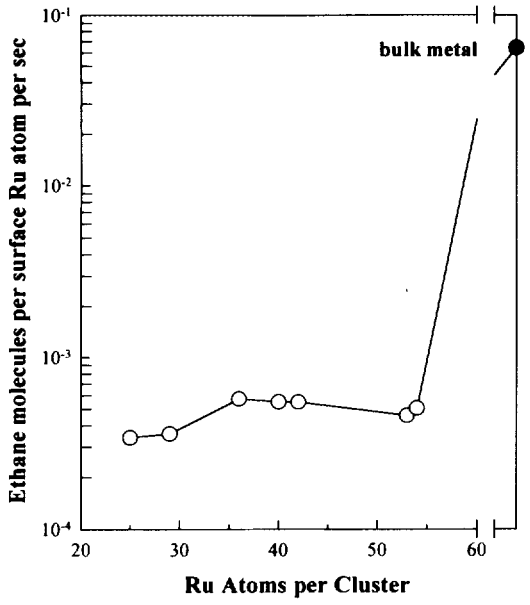

FIG. 4. Catalytic activity of Ru/NaY for ethane hydrogenolysis reaction, plotted as a function of the number of Ru atoms per cluster estimated from the xenon adsorption. Open circles represent Ru clusters in supercage. The filled circle represents the 100 nm × 20 nm Ru agglomerate located on the external surface of NaY (4).

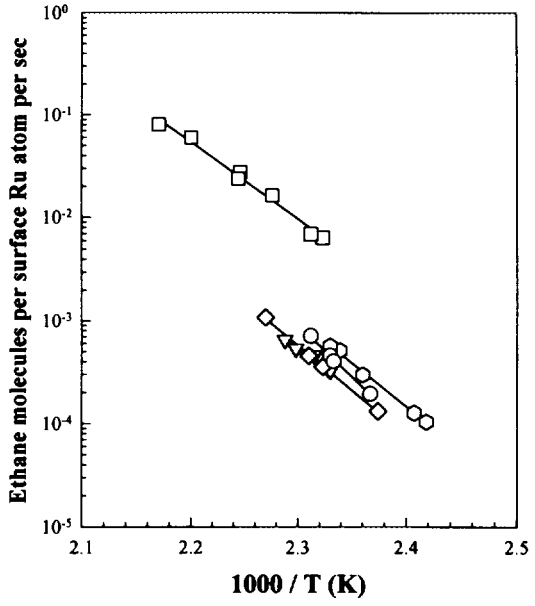

FIG. 5. Arrhenius plot for ethane hydrogenolysis reaction on Ru/NaY: (□) 100 nm × 20 nm Ru agglomerate on the external surface of NaY; (◇) (Ru clusters trapped in the supercage of NaY with) 29, (○) 36 and (○) 53 Ru atoms per cluster as estimated from xenon adsorption, respectively; (▽) 3.0 wt% Ru/NaY taken from Ref. (11).

surface Ru atom that is exposed through an aperture of the supercage. Space-filling models have been used to estimate the number of surface atoms. The ratio of surface atoms to total atoms in each cluster is included in Table 1.

The catalytic activity of Ru/NaY clusters located in the supercage was smaller by two orders of magnitude than that for large Ru particles located on the external surface of zeolite. However, no distinct difference could be found between the small clusters trapped in the supercage. Transmission electron micrographs of Ru/NaY taken after ethane hydrogenolysis reaction showed small Ru clusters trapped in the supercage similar to that before reaction, which indicated that there was neither gross sintering nor cluster growth during the reaction. Arrhenius plots for the ethane hydrogenolysis rate over Ru/NaY are shown in Fig. 5. The activation energies of the reaction, determined from the slopes in the Arrhenius plots for the small Ru clusters, all fall within a range of 39.6 kcal · mol^{-1} (±5.3) within a 99% confidence limit. This range of activation energy includes 35 kcal · mol^{-1}, which was determined for large Ru metal particles located on the external surface of zeolite in the present work, and also other results reported by Sajkowski *et al.* (11).

XANES

Figures 6 and 7 show XANES spectra for the Ru/NaY samples measured in H_2 at the Ru *K* edge. In Fig. 6, XANES of the Ru cluster consisting of 48 Ru atoms

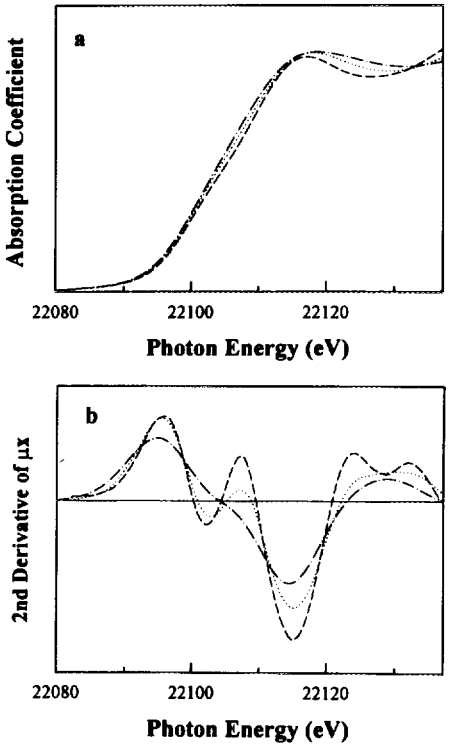

FIG. 6. (a) X-ray absorption near edge structure of Ru/NaY and (b) its second derivative above the Ru *K* edge: (---) 100 nm × 20 nm Ru metal agglomerate sintered by heating in O_2 at 573 K (4); (-·-·-) Ru cluster consisting of 48 Ru atoms entrapped in NaY supercage; (···) Ru/NaY sintered by heating in O_2 at 473 K.

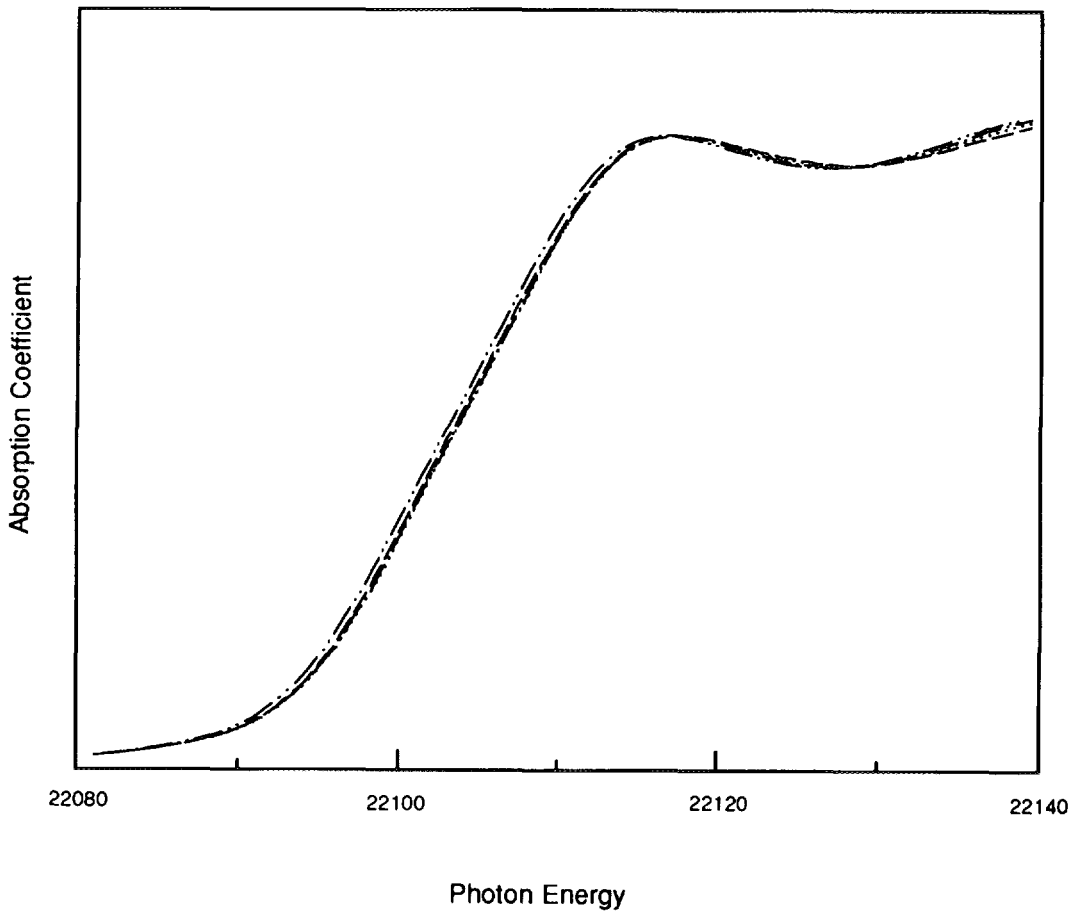

FIG. 7. X-ray absorption near edge structure of Ru/NaY above the Ru K edge: (—) 22; (---) 33; (···) 40; (-·····) 48 Ru atoms per cluster estimated using xenon adsorption, respectively.

trapped in a NaY supercage shows an edge shift of about 4.4 eV from the absorption edge of large Ru particles (100 nm × 20 nm) supported on the external surface of the NaY crystal (4). An additional difference between the small Ru clusters and the large Ru particles was the disappearance of an edge shoulder at 22.102 keV in the case of small clusters. The edge shoulder was due to a $4d$–$5p$ hybridization that enables the dipole-forbidden transition from $1s$ to $4d$ orbitals to occur effectively. The $1s \rightarrow 4d$ transition became very weak in the case of small Ru clusters, indicating that the electron was donated from chemisorbed hydrogen into the $5p$ orbital of Ru. However, Fig. 7 shows that the XANES did not change further as the Ru cluster size varied in the supercage. Thus, the XANES did not indicate any electronic effects coming from the cluster size change within the supercage.

DISCUSSION

Before discussing the effect of cluster size on reaction rates, it is first necesasry to address the precision and accuracy of the xenon adsorption technique used to determine the number of Ru atoms per cluster. The precision was better than ±5%. But the accuracy should be considered very carefully, since the xenon adsorption technique is based on some assumptions (3–8). For this reason, we have measured EXAFS of the Ru/NaY clusters under the same conditions as those for XANES, and performed the curve-fitting analysis using the large Ru particles supported on the external surface of zeolite crystal as reference. The Ru–Ru coordination number (N) is plotted against the number of Ru atoms per cluster in Fig. 8 (12, 13).

The solid curve in Fig. 8 shows experimental data points obtained from EXAFS curve fitting. The dotted line represents the theoretical coordination number for a cluster model consisting of balls packed together in a face-centered cubic way to give a geometry as near as possible to that of a sphere. Narrow scattering of the experimental data points around the solid curve indicates a good correlation between the N from the EXAFS experiment and the number of Ru atoms from the xenon adsorption mea-

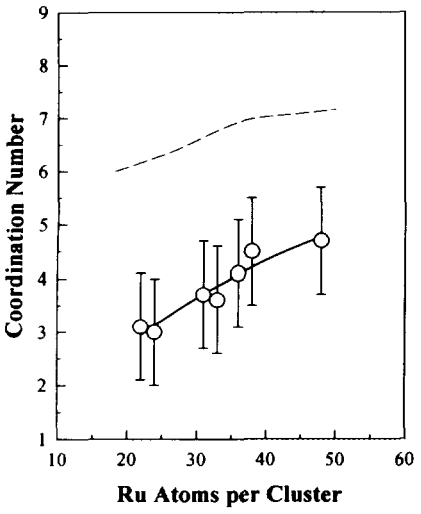

FIG. 8. The Ru–Ru coordination number plotted as a function of the average number of Ru atoms per cluster for Ru/NaY obtained from xenon adsorption: (---) theoretical coordination number obtained from space filling model; (○) coordination number obtained from EXAFS curve fitting; and (—) fitted line for data points of (○).

surement. Thus, the results confirm the good precision of the xenon adsorption technique.

Interestingly, the experimental data were lower than the theoretical curve throughout the entire range in Fig. 8. Either the results from EXAFS underestimated–or the results from xenon adsorption overestimated N. The standard curve-fitting method used for the present EXAFS may considerably underestimate N for very small clusters due to asymmetric disorder and anharmonic vibration (14, 15). It is also possible that the shape of the cluster may substantially differ from the assumed sphere as in the case of Ru and Ir clusters on silica (16), or some Ru atoms may be located inside the sodalite cage. It may be stated that the actual Ru cluster size was not larger than the size estimated by the xenon adsorption technique. Comparison of the xenon adsorption results with EXAFS at low temperatures, including more elaborate data analysis of other Group 8 metal clusters under He and H_2 atmosphere, is necessary to understand the discrepancy in further detail (13).

Recent studies of XANES at L_{II} and L_{III} edges of the third-row transition metals indicate a significant change in the electronic structure of small metal clusters trapped in the supercage of Y zeolite, probably due to decreases in the metal cluster size (17, 18). Particularly noteworthy are increases in white line height of XANES at the Pt L_{III} edge and in the $5d_{5/2}$ bandwidth of Pt clusters in zeolite (19). The nearest Pt–Pt pair distance is also known to decrease in metal clusters compared with the bulk metal (20, 21). Moreover, these peculiar properties of small clusters were markedly affected by hydrogen chemisorption. For example, the lattice structure of Pt/NaY relaxed to a bulk-like structure after hydrogen chemisorption (19–21). Electron transfer occurred from hydrogen to the $5d_{5/2}$ band of clusters. In comparison, less detailed information on the cluster size effect can be obtained from XANES at K edges because the core level excitation is not very sensitive to the chemical state (22–24). Davis *et al.* (25) reported a K-edge shift from a small Pd cluster supported on γ-alumina. A shoulder at the Pd edge also disappeared, similar to the results for Ru/NaY shown in Fig. 6.

The metal dispersion (i.e., percent metal exposed to the surface) changes only to a small extent, around 80–100%, even if the number of metal atoms per cluster is increased threefold, from 20 to 60. This means that some physical properties due to the contribution from surface atoms may not change very much over this range while other properties coming from the intrinsic size effect may appear to change more clearly. Therefore, the minor changes of XANES shown in Fig. 7 suggest that the changes in Fig. 6 can be attributed mostly to a surface-like property of the small Ru cluster in zeolite. Thus, the intrinsic size effects on the electronic property was not detected for these small Ru clusters.

Catalytic hydrogenolysis of alkane has been widely used as a probe reaction to investigate the dependence of catalytic activity on cluster size (26–33). Lam and Sinfelt reported a decrease in catalytic activity of cyclohexane hydrogenolysis due to the loss of multiple active sites as the Ru dispersion increased (26). Foger and Anderson concluded that an active site of iridium catalyst for *n*-butane and neo-hexane hydrogenolysis consisted of two nearest Ir atoms (27). A similar conclusion was drawn by Burton and Hyman in the case of ethane hydrogenolysis over nickel catalyst (28). Galvagno *et al.* (29) studied ethane hydrogenolysis over Ru clusters of different sizes supported on different supports, but obtained no direct correlation between the catalytic activity and the metal particle size. Sajkowski *et al.* (11) reported that the catalytic activity of Ru clusters supported on Y zeolite for cyclopropane hydrogenolysis was significantly affected by the metal dispersion. In the present study, the catalytic activity for ethane hydrogenolysis was very similar for all small clusters trapped in the supercage. The activation energy of reaction listed in Table 2 also did not change with the Ru cluster size.

It may be assumed that ethane is chemisorbed in the first step of the reaction with dissociation of the carbon–hydrogen bonds, ultimately yielding a hydrogen-deficient surface species, C_2H_x (27). In this case, the reaction intermediate requires a site comprising an ensemble of adjacent surface Ru atoms. As the number of the constituent atoms in a Ru cluster decreases to only 20 atoms, the surface concentration of the ensembles to accommo-

date the intermediate will then sharply decline since a large fraction of the surface atoms exist at edges and corners. Therefore, ethane hydrogenolysis activity of such small Ru clusters can be much lower than that of large Ru metal particles.

CONCLUSIONS

In the present work, a series of Ru/NaY samples was obtained with different cluster sizes. The number of Ru atoms per cluster was estimated by xenon adsorption, and the average values ranged from 20 to 60 depending on the preparation conditions. All XANES spectra taken at the Ru *K* edge under H_2 atmosphere were very similar to each other within this cluster size range. However, the XANES spectra were markedly different from the bulk metal data, and this was attributed to a difference in metal dispersion.

The small Ru clusters exhibited a catalytic activity per surface atom for ethane hydrogenolysis that was two orders of magnitude smaller than those obtained from large Ru metal agglomerates. However, there was no indication of a cluster size dependence of the catalytic activity within the small Ru clusters inside the supercage. Moreover, there appeared to be no considerable changes in the activation energy due to the cluster size change. These results led us to attribute the weak catalytic activity of the small Ru clusters mostly to an ensemble effect, due to decreases in the number of available catalytic activity sites on the Ru surface planes. Nevertheless, it is interesting that a very small Ru cluster consisting of at most 20 Ru atoms still showed an appreciable activity for heterogeneous catalytic reaction.

ACKNOWLEDGMENTS

This research was supported by the Korea Science and Engineering Foundation (1991–1993). The authors are grateful for support from the Photon Factory (Proposal 92G193) and the Pohang Accelerator Laboratory for XAFS.

REFERENCES

1. Sachtler, W. M. H., and Zhang, Z., *Adv. Catal.* **39,** 129 (1993).
2. Che, M., and Bennett, C., *Adv. Catal.* **36,** 55 (1989).
3. Ryoo, R., Cho, S. J., Pak, C., Kim, J.-G., Ihm, S.-K., and Lee, J. Y., *J. Am. Chem. Soc.* **114,** 76 (1992).
4. Cho, S. J., Jung, S. M., Shul, Y. G., and Ryoo, R., *J. Phys. Chem.* **94,** 9922 (1992).
5. Ryoo, R., Cho, S. J., Pak, C., and Lee, J. Y., *Catal. Lett.* **20,** 107 (1993).
6. Kim, J.-G., Ihm, S.-K., Lee, J. Y., and Ryoo, R., *J. Phys. Chem.* **95,** 8546 (1991).
7. Ihee, H., Bécue, T., Ryoo, R., Potvin, C., Manoli, J.-M., and Djéga-Mariadassou, G., *in* "Zeolite and Related Microporous Materials: State of the Art 1994" Weitkamp, J., Karge, H. G., Pfeifer, H. and Hölderich, W. (Eds.), Studies in Surface Science and Catalysis, Vol. 84, p. 765. Elsevier, Amsterdam, 1994.
8. Pak, C., Cho, S. J., Lee, J. Y., and Ryoo, R., *J. Catal.* **149,** 61 (1994).
9. Madhusudhan, C. P., Patil, M. D., Good, M. L., *Inorg. Chem.* **18,** 2384 (1979).
10. Schlatter, J. C., and Boudart, M., *J. Catal.* **24,** 482 (1972).
11. Sajkowski, D. J., Lee, J. Y., Schwank, J., Tian, Y., and Goodwin, J. R., *J. Catal.* **97,** 549 (1986).
12. (a) The curve fit of EXAFS spectrum above the Ru *K* edge for Ru/NaY sample was carried out with UWXAFS 2. (b) Frenkel, A. I., Stern, E. A., Qian, M., and Newville, M., *Phys. Rev. B* **48,** 12449 (1993).
13. Cho, S. J., and Ryoo, R., in preparation.
14. Clausen, B. S., Grabæk, L., Topsøe, H., Hansen, L. B., Stoltze, P., Nørskov, J. K., and Nielsen, O. H., *J. Catal.* **141,** 368 (1993).
15. Bunker, G., *Nucl. Instrum. Methods Phys. Rev.* **207,** 437 (1983).
16. Ashcroft, A. T., Cheetham, A. K., Harris, P. J. F., Jones, R. H., Natarajan, S., Sankar, G., Stedman, N. J., and Thomas, J. M., *Catal. Lett.* **24,** 47 (1994).
17. Samant, M. G., and Boudart, M., *J. Phys. Chem.* **95,** 4070 (1991).
18. Boudart, M., Samant, M. G., and Ryoo, R., *Ultramicroscopy* **20,** 125 (1986).
19. Kim, J. M., and Ryoo, R., in preparation.
20. Moraweck, B., Clugnet, G., and Renouprez, A. J., *Surf. Sci.* **81,** L631 (1979).
21. Koningsberger, D. C., and Sayers, D. E., *Solid State Ionics* **16,** 23 (1985).
22. Sham, T. K., *Phys. Rev. B* **31,** 1903 (1985).
23. McCaulley, J. A., *J. Phys. Chem.* **97,** 10372 (1993); McCaulley, J. A., *Phys. Rev. B* **47,** 4873 (1993).
24. Moraweck, B., Renouprez, A. J., Hlil, E. K., and Baudoing-Savois, R., *J. Phys. Chem.* **97,** 4288 (1993).
25. Davis, R. J., Landry, S. M., Horsely, J. A., and Boudart, M., *Phys. Rev. B* **39,** 10580 (1989).
26. Lam, Y. L., and Sinfelt, J. H., *J. Catal.* **42,** 319 (1976).
27. Foger, K., and Anderson, J. R., *J. Catal.* **59,** 325 (1979).
28. Burton, J. J., and Hyman, E., *J. Catal.* **37,** 114 (1975).
29. Galvagno, S., Schwank, J., Gubitosa, G., and Tauszik, G. R., *J. Chem. Soc. Faraday Trans. 1* **78,** 2509 (1982).
30. Yates, D. J. C., and Sinfelt, J. H., *J. Catal.* **8,** 348 (1967).
31. Carter, J. L., Cusumano, J. A., and Sinfelt, J. H., *J. Phys. Chem.* **70,** 2257 (1966).
32. Sinfelt, J. H., Carter, J. L., and Yates, D. J. C., *J. Catal.* **24,** 283 (1972).
33. Sinfelt, J. H., *Catal. Lett.* **9,** 159 (1991).